Int. J. Electrochem. Sci., 11 **(2016)** 8654 – 8661, doi: 10.20964/2016.10.14

International Journal of
ELECTROCHEMICAL
SCIENCE
www.electrochemsci.org

Synthesis of Fe_2O_3/Graphene Composite Anode Materials with Good Cycle Stability for Lithium-ion Batteries

Lilai Liu[*], *Zhiwei Song, Juan Wang, Lu Shen, Bangdi Tu, Sucheng Wang, Daorui Mao*

College of Environmental and Chemical Engineering, Heilongjiang University of Science and Technology, Harbin 150022, China
[*]E-mail: lllusth@163.com

Received: 3 April 2016 / *Accepted:* 26 July 2016 / *Published:* 6 September 2016

Fe_2O_3/graphene composite anode materials have been successfully synthesized by a PVP-assisted homogeneous precipitation method. The size of Fe_2O_3 nanoparticles on the surface of graphene sheets was less than 35 nm. Fe_2O_3 nanoparticles and graphene sheets formed a network structure. Electrochemical properties were evaluated in two-electrode cells versus metallic lithium. The Fe_2O_3/graphene composite exhibited excellent electrochemical lithium storage performances. The first discharge and charge capacities were 1600 and 1053 mA h g^{-1} at a current density of 100 mA g^{-1}, and the first coulomb efficiencies was 65.8%. The reversible specific capacity remained 893 mA h g^{-1} and the capacity retention was 84.8% after 100 cycles.

Keywords: Fe_2O_3; graphene; composite; anode; lithium-ion batteries

1. INTRODUCTION

Lithium-ion batteries (LIBs) as a promising electrochemical power source have attracted great interest [1]. The applications of LIBs have been extended to aerospace and hybrid vehicle domain from portable electronic gradually [2]. As a result, the high energy density batteries are more and more required. As the major anode material of commercial LIBs, graphite has excellent electrochemical properties and low cost. However, it has a low theoretical capacity of 372 mA h g^{-1}, which cannot meet future requirements of power LIBs [3]. Therefore, the new alternative anode materials with higher performances are desired. The theoretical capacity of Fe_2O_3 is 1005 mA h g^{-1}, and Fe_2O_3 has the characteristics of low processing cost and environment friendly. Therefore, it is widely attracted significant research attention [4-6]. However, Fe_2O_3 used as an anode material for LIBs will suffer from poor cycle performance, because it will agglomerate and happen huge volume change in the

process of charging and discharging [7]. To improve the charge-discharge properties and cycle performances of Fe_2O_3 electrodes, composite anode materials have been widely considered. Carbon nanofibers, carbon nanotubes and graphene have high electronic conductivity, excellent buffering effect and mechanical strength, which have been introduced into Fe_2O_3 composite anode materials [8-10]. Graphene has been widely studied due to its theoretical lithium storage capacity of 744 mA h g^{-1} and unique properties [11]. Graphene not only possesses stable structure, but also has the characteristics of high specific surface area (~2600 m^2 g^{-1}) and excellent electronic conductivity (~6000 S cm^{-1}) [12-14]. Fe2O3/graphene composite as anode materials for LIBs have been reported, however the cycling performances of Fe_2O_3/graphene electrode for LIBs need to be improved [15-17]. Herein, we reported a facile PVP-assisted homogeneous precipitation synthesis method of Fe_2O_3/graphene composite. The electrochemical performances of Fe_2O_3/graphene composite anode material for LIBs were studied and compared with that of pure Fe_2O_3 nanoparticles and graphene sheets.

2. EXPERIMENTAL

2.1 Preparation of materials

Graphite oxide was prepared by the modified Hummers method as we reported previously [18]. The 2 mg mL^{-1} graphite oxide aqueous solution was handled by ultrasonic for 1 h to prepare graphene oxide. The Fe_2O_3/graphene composite was prepared by a PVP-assisted homogeneous precipitation method. In a typical reaction, 0.512 g ferric nitrate, 2.268 g urea solution, and 0.5 g PVP was added to 100 mL graphene oxide aqueous solution in turn, then ultrasonic treatment for 30 min. Put the graphene oxide supernatant solution into a reaction system and reacted 1.5 h at 90 ^oC. Washed sample using deionized water and ethanol for several times by centrifugation and freeze-dried overnight. The dried sample was heat-treated at 500 ^oC for 2 h in N_2. Fe_2O_3/graphene composite was finally obtained. As comparison, pure Fe_2O_3 was prepared under the same conditions without the addition of graphene oxide supernatant solution. The graphene sheets was prepared under the same conditions without the addition of ferric nitrate and urea.

2.2 Materials characterizations and electrochemical measurements.

The structures of the as-prepared materials were characterized by X-ray diffraction (XRD, Bruker D8 Advance). The morphologies were characterized by scanning electron microscopy (SEM, QUANTA 200F) and transmission electron microscopy (TEM, FEI TECNAI G2 F20). Electrochemical measurements were carried out using CR2025 coin-type cells. Fe_2O_3/graphene composite was the active material of working electrode, and the mass ratio of active material, polyvinylidene fluoride and acetylene black was 8:1:1. The galvanostatic charge and discharge curves of cells were measured by a battery testing system (Neware Electronic Co.) at different current densities. Cyclic voltammetry (CV) curves and electrochemical impedance spectroscopy (EIS) data were recorded by an electrochemistry working station (AUTOLAB PGSTAT302).

3. RESULTS AND DISCUSSION

The structures of products were analyzed by XRD. Figure 1 shows the XRD patterns of graphene oxide, graphene sheets, pure Fe_2O_3 nanoparticles and Fe_2O_3/graphene composite. The diffraction peaks at ~11^o can be attributed to (002) of the graphene oxide [19]. The diffraction peaks of Fe_2O_3 nanoparticles are clearly distinguishable. All strong diffraction peaks are consistent with (012), (104), (110), (113), (024), (018), (214) and (300) of hematite crystalline Fe_2O_3 phase (JCPDS card no. 33-0664). Graphene oxide diffraction peaks are not observed in the Fe_2O_3/graphene composite, indicating that graphene oxide is reduced to graphene. And no diffraction peaks of graphene sheets are observed, indicating that the graphene sheets are completely exfoliated and the diffraction peaks of graphene are covered by those of Fe_2O_3 [20].

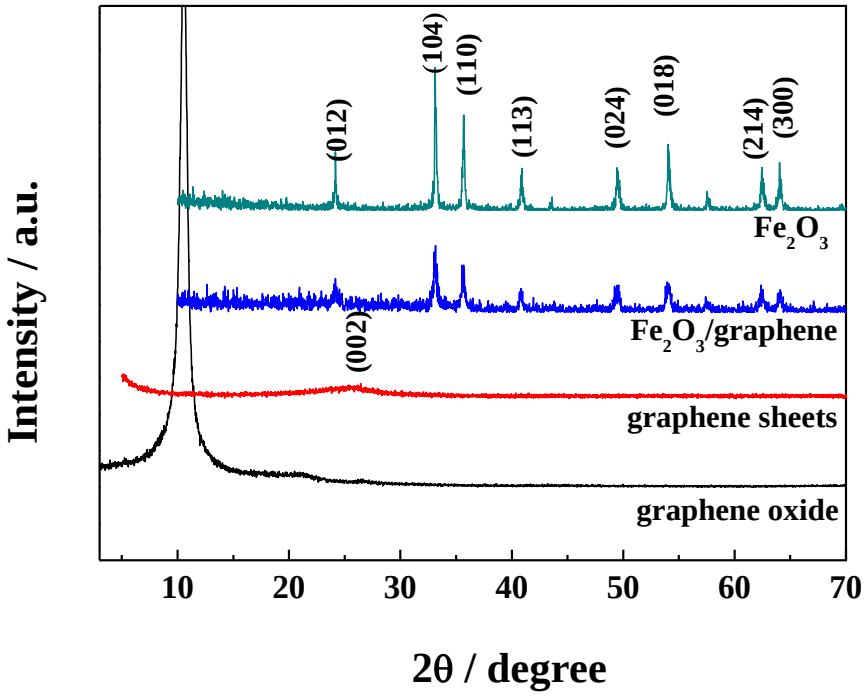

Figure 1. XRD patterns of graphene oxide, graphene sheets, Fe_2O_3 nanoparticles and Fe_2O_3/graphene

Figure 2 shows the morphologies and structures of graphite oxide, graphene sheets, pure Fe_2O_3 nanoparticles and Fe_2O_3/graphene composite. From figure 2 (a), we can see that there are many folds on the surface of graphite oxide sheets. Figure 2 (b) shows graphene sheets are composed of many thinner transparent sheets, which implies the graphene sheets are only a few layers. Figure 2 (c) shows TEM image of Fe_2O_3 nanoparticles prepared using PVP-assisted homogeneous precipitation method, and the average particle diameter of Fe_2O_3 nanoparticles is about 40 nm. The TEM image of Fe_2O_3/graphene composite in figure 2 (e) reveals that the graphene sheets is decorated with Fe_2O_3 nanoparticles on the basal plane. The Fe_2O_3 nanocrystals are in the diameters ranging from 25~30 nm, uniformly anchored on the surface of graphene sheets. From the HRTEM images in figure 2 (d) and (f), the interplanar distance of 0.25 nm can be identified as d (110) of Fe_2O_3 nanoparticles [21].

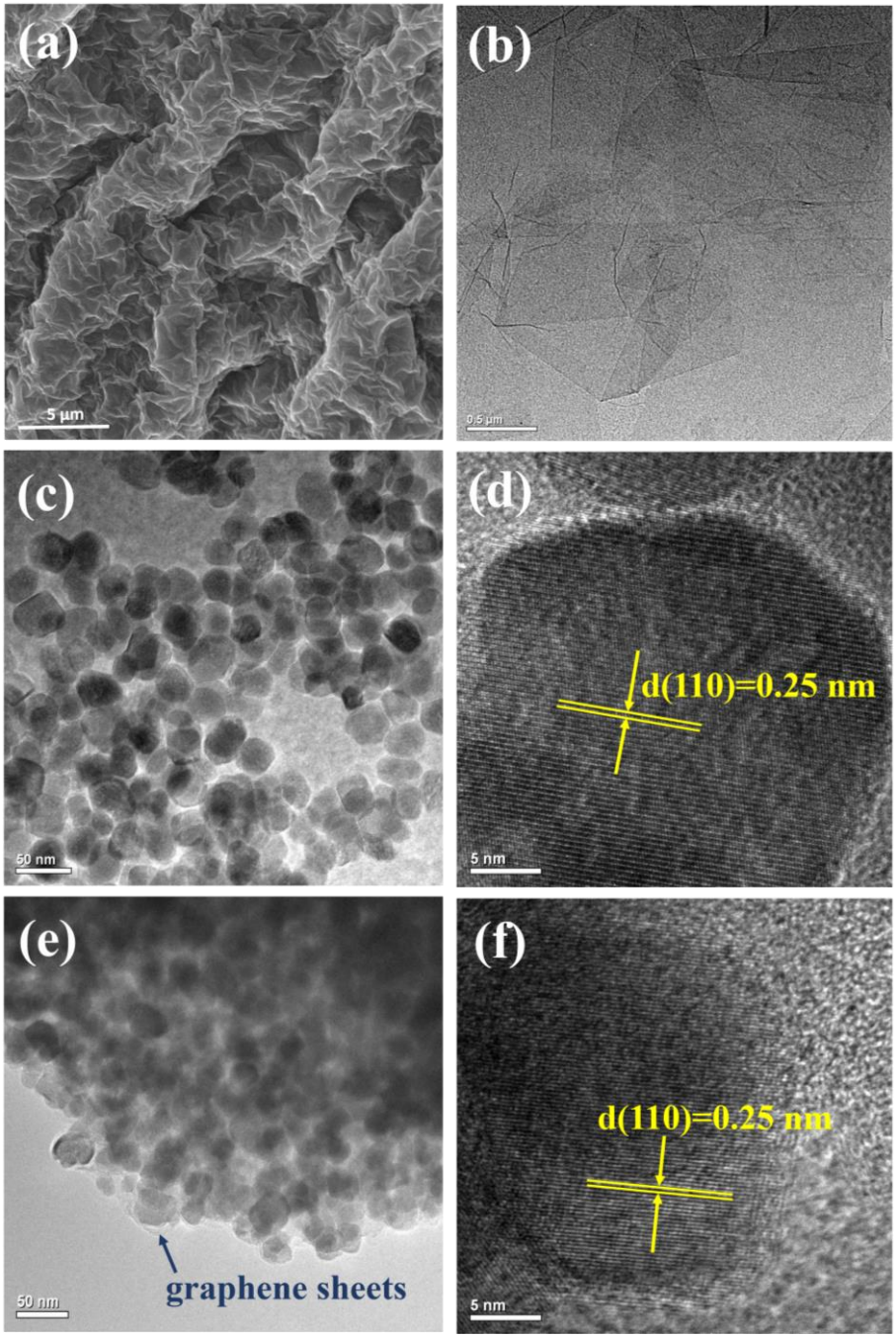

Figure 2. SEM image of (a) graphite oxide, TEM image of (b) graphene sheets, TEM image (c) Fe_2O_3 and (e) Fe_2O_3/graphene, HRTEM images of (d) Fe_2O_3 and (f) Fe_2O_3/graphene

A series of electrochemical measurements were performed to study the lithium storage capabilities of the Fe_2O_3/graphene composite. The CV curves of the Fe_2O_3/graphene composite at a scan rate of 0.1 mV s^{-1} are shown in figure 3. In the first cycle, there are two peaks at 0.01 and 0.75 V in the cathodic polarization process, which should be attributed to the formation of a series of LiC_6 and reduction of Fe_2O_3 [22]. Meanwhile, there are two peaks at 1.67 and 1.92 V in the anodic polarization process, which can be ascribed to iron oxide into bivalent iron and continue to be oxidized to ferric iron. The peak at 0.75 V is corresponding to the first discharge voltage plateau. After the first cycle,

the CV curves of the Fe_2O_3/graphene composite are almost completely overlap, which revealing the Fe_2O_3/graphene composite has an excellent reversibility.

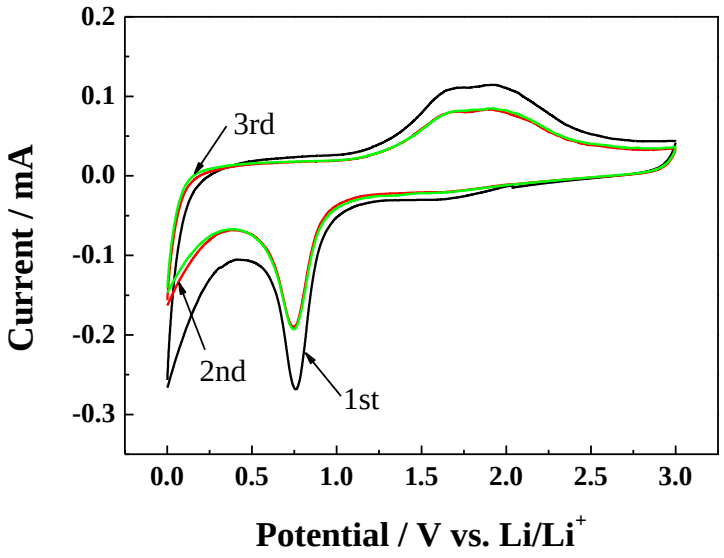

Figure 3. CV curves of different cycles of the Fe_2O_3/graphene composite at 0.1 mV s^{-1}

The lithium storage performances of pure Fe_2O_3 nanoparticles, graphene sheets and Fe_2O_3/graphene composite as anode materials were tested. The different cycling discharge-charge curves of pure Fe_2O_3 nanoparticles and Fe_2O_3/graphene composite were shown in figure 4. The test current density was 100 mA g^{-1}, and the voltage range was 3.0~0.01 V. Figure 4 shows the first discharge and charge specific capacities of Fe_2O_3 are 1502 and 898 mA h g^{-1}, respectively. By comparison, the discharge and charge specific capacities of Fe_2O_3/graphene are 1600 and 1053 mA h g^{-1}, respectively. The first coulomb efficiency of Fe_2O_3/graphene is 65.8% and higher than that of Fe_2O_3. In addition, there is an obvious voltage platform in the discharge curve in the first discharge process of Fe_2O_3/graphene composite, which is consistent with the result of CV measurement.

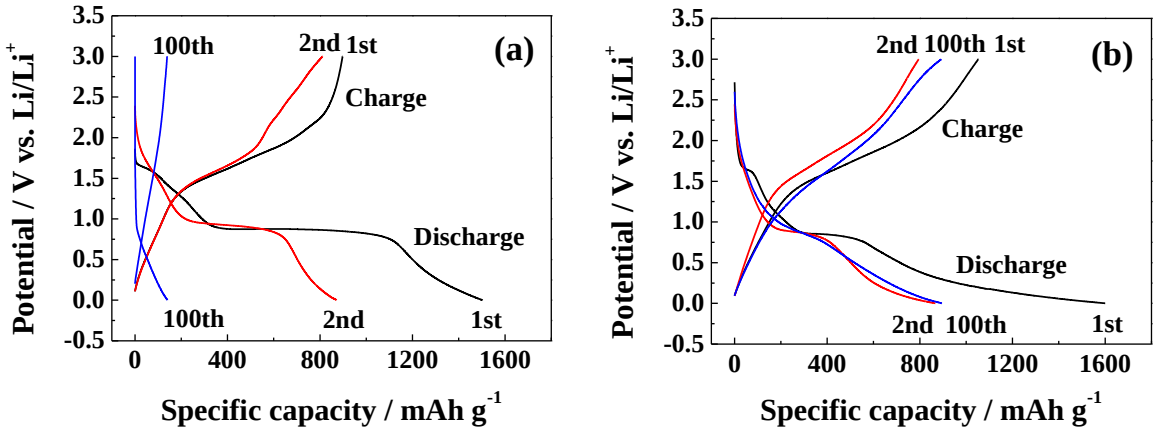

Figure 4. Galvanostatic discharge/charge profiles for different cycles: (a) Fe_2O_3 and (b) Fe_2O_3/graphene composite

The voltage platform corresponds to the formation of Fe and Li_2O, which is a conversion reaction between Fe_2O_3 and Li^+. The large irreversible capacity losses during the first cycle is related to the decomposition of electrolyte forming a sold-electrolyte interface (SEI) [23]. In the second cycle, the coulombic efficiency of Fe_2O_3/graphene increased to 91.7% and the specific discharge capacity maintained 876 mA h g^{-1}.

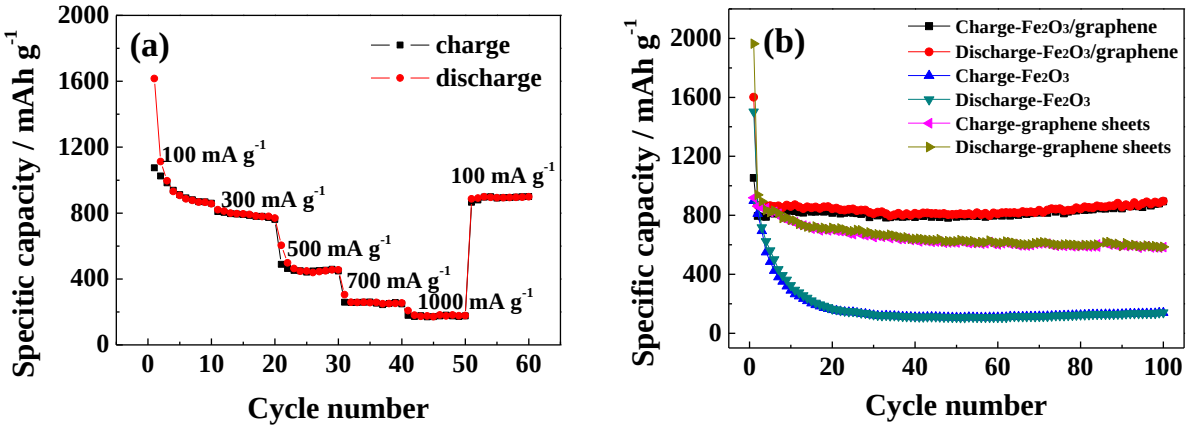

Figure 5. (a) Rate capability from 100 to 1000 mA g^{-1}; (b) Cycling performances of Fe_2O_3, graphene sheets and Fe_2O_3/graphene composite

The rate performance and cycling performances of materials are shown in figure 5. The Fe_2O_3/graphene composite has a good rate capability, as shown in figure 5 (a). The reversible specific capacities of Fe_2O_3/graphene composite are 859, 761, 448, 249 and 175 mA h g^{-1} at the current densities of 100, 300, 500, 700 and 1000 mA g^{-1}, respectively. A reversible capacity of 890 mA h g^{-1} is achieved after the rate changed back to 100 mA g^{-1}. Moreover, the reversible specific capacity of Fe_2O_3/graphene composite presents a slight increase when the current density changes back from 1000 to 100 mA g^{-1}. The cycling performances of Fe_2O_3, graphene sheets and Fe_2O_3/graphene composite are shown in figure 5 (b). We can see that the discharge-charge specific capacities slightly decrease at the initial cycles, but a slight increase after 31th cycles. The reversible specific capacity is 894 mA h g^{-1} after 100 cycles at 100 mA g^{-1}, and the capacity retention is 84.8%. It is obvious that the cycling performance of Fe_2O_3/graphene composite is better than that of graphene sheets and Fe_2O_3 nanoparticles. The smaller size of Fe_2O_3 nanoparticles, the network microstructure of Fe_2O_3/graphene, and the synergy between Fe_2O_3 nanoparticles and graphene sheets are primary reason of the better electrochemical performances of Fe_2O_3/graphene composite. Fe_2O_3 nanoparticles can prevent the stack of graphene sheets, and graphene sheets can prevent the agglomeration and volume expansion/contraction of Fe_2O_3 nanoparticles. On the other hand, the network structure of Fe_2O_3/graphene composite is a highly conductive matrix, which can ensure the stability contact and improve the electrical conductivity of electrode materials.

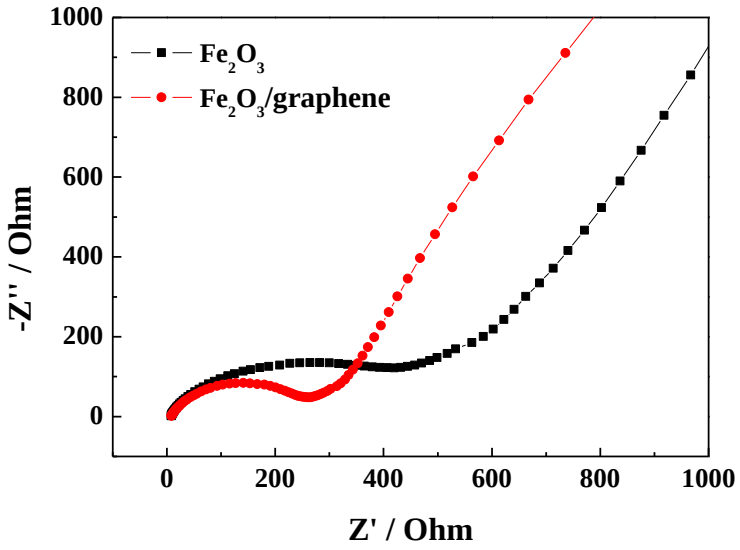

Figure 6. Nyquist plots of Fe_2O_3 and Fe_2O_3/graphene composite after the first discharge/charge cycle

The EIS for Fe_2O_3 and Fe_2O_3/graphene composite was further compared. Figure 6 shows the nyquist plots of Fe_2O_3 and Fe_2O_3/graphene composite after the first discharge and charge cycle. The nyquist plots is composed of two semicircles at high-frequency and medium-frequency regions and a linear part at the low-frequency end. The semicircle in medium-frequency region is assigned to charge-transfer impedance and the constant phase element of the electrode/electrolyte interface [24]. It is obviously that the semicircle radius of Fe_2O_3/graphene is much smaller than that of the Fe_2O_3, indicating charge transfer resistance of Fe_2O_3/graphene composite is lower than Fe_2O_3, which further illustrate the addition of graphene sheets improved the electronic conductivity of Fe_2O_3/graphene composite.

4. CONCLUSIONS

Fe_2O_3/graphene composite was successfully synthesized by a PVP-assisted homogeneous precipitation method. The preparation method is more simple and controllable. The Fe_2O_3/graphene composite electrode exhibited better performances of lithium storage compared with the Fe_2O_3 and graphene sheets. The smaller size of Fe_2O_3 nanoparticles, the network microstructure of Fe_2O_3/graphene, and the synergy between Fe_2O_3 nanoparticles and graphene sheets are primary reason of the better electrochemical performances of Fe_2O_3/graphene composite.

ACKNOWLEDGEMENT

The work is supported by Science and Technology Research Project of the Heilongjiang Province Department of Education (no. 12531587).

References

1. G. Jeong, Y. Kim, H. Kim, H. Sohn, *Energy Environ. Sci.*, 4 (2011) 1986.

2. J. B. Goodenough and Y. Kim, *Chem. Mater.*, 22 (2010) 587.
3. B. Scrosati and J. Garche, *J. Power Sources*, 195 (2010) 2419.
4. P. Poizot, S. Laruelle, S. Grugeon, L. Dupont and J-M. Tarascon, *Nature*, 407 (2000) 496.
5. H. Liu, G. Wang, J. Park, J. Wang, H. Liu and C. Zhang, *Electrochim. Acta*, 54 (2009) 1733.
6. L. Yang, Q. Gao, Y. Zhang, Y. Tang and Y. Wu, *Electrochem. Commun.*, 10 (2008) 118.
7. J. Chen, L. Xu, W. Li and X. Gou, *Adv. Mater.*, 17 (2005) 582.
8. B. Huang, S. Okada and J. Yamaki, *J. Power Sources*, 178 (2008) 402.
9. B. Huang, I. Watanabe, T. Doi, S. Okada and J. Yamaki, *J. Power Sources*, 161 (2006) 1281.
10. X. Zhu, Y. Zhu, S. Murali, M. Stoller and R.S. Ruoff, *ACS Nano*, 5 (2011) 3333.
11. P. Guo, H. Song and X. Chen, *Electrochem. Commun.*, 11 (2009) 1320.
12. A. K. Geim, *Nature*, 324 (2009) 1530.
13. C.T.J. Low, F.C. Walsh, M.H. Charkrabarti, M.A. Hashim and M.A. Hussain, *Carbon*, 54 (2013) 1.
14. A.A. Balandin, S. Ghosh, W. Bao, I. Calizo, D. Teweldebrhan, F. Miao and C.N. Lau, *Nano Lett.*, 8 (2008) 902.
15. G. Wang, T. Liu, Y. Luo, Y. Zhao, Z. Ren, J. Baic and H. Wang, *J. Alloy. Compd.*, 509 (2011) L216.
16. Y. Zou, J. Kan and Y. Wang, J. Phys. Chem. C, 115 (2011) 20747.
17. M. Zhang, B. Qu, D. Lei, Y. Chen, X. Yu, L. Chen, Q. Li, Y. Wang and T. Wang, J. Mater. Chem., 22 (2012) 3868.
18. L. Liu, M. An, P. Yang and J. Zhang, *Int. J. Electrochem. Sci.*, 10 (2015) 1582.
19. D. Pan, S. Wang, B. Zhao, M. Wu, H. Zhang and Y. Wang, *Chem. Mater.*, 21 (2009) 3136.
20. L. Xiao, D. Wu, S. Han, Y. Huang, S. Li, M. He, F. Zhang and X. Feng, *ACS Appl. Mater.* Interfaces, 5 (2013) 3764.
21. J. Qu, Y. Yin, Y. Wang, Y. Yan, Y. Guo and W. Song, *ACS Appl. Mater. Interfaces*, 5 (2013) 3932.
22. G. Wang, H. Wang, S. Cai, J. Bai, Z. Ren and J. Bai, *J. Power Sources*, 239 (2013) 37.
23. W. Zhou, Y. Y. Tay, X. Jia, D. Y. Y. Wai, J. Jiang, H. H. Hoon and T. Yu, *Nanoscale*, 4 (2012) 4459.
24. L. Tian, Q. Zhuang, J. Li, C. Wu, Y. Shi and S. Sun, *Electrochimica Acta*, 65 (2012) 153.